

Article

Integrating Physics and Data Driven Cyber-Physical System for Condition Monitoring of Critical Transmission Components in Smart Production Line

Lin Song ¹ , Liping Wang ^{1,2}, Jun Wu ^{2,*}, Jianhong Liang ² and Zhigui Liu ¹

¹ College of Information Engineering, Southwest University of Science and Technology, Mianyang 621000, China; songlin606060@163.com (L.S.); lpwang@mail.tsinghua.edu.cn (L.W.); liuzhigui@swust.edu.cn (Z.L.)

² State Key Laboratory of Tribology and Institute of Manufacturing Engineering, Department of Mechanical Engineering, Tsinghua University, Beijing 100084, China; jianhong4337@163.com

* Correspondence: jhwu@mail.tsinghua.edu.cn; Tel.: +86-010-62772633

Abstract: In response to the lack of a unified cyber–physical system framework, which combined the Internet of Things, industrial big data, and deep learning algorithms for the condition monitoring of critical transmission components in a smart production line. In this study, based on the conceptualization of the layers, a novel five-layer cyber–physical systems framework for smart production lines is proposed. This architecture integrates physics and is data-driven. The smart connection layer collects and transmits data, the physical equation modeling layer converts low-value raw data into high-value feature information via signal processing, the machine learning modeling layer realizes condition prediction through a deep learning algorithm, and scientific decision-making and predictive maintenance are completed through a cognition layer and a configuration layer. Case studies on three critical transmission components—spindles, bearings, and gears—are carried out to validate the effectiveness of the proposed framework and hybrid model for condition monitoring. The prediction results of the three datasets show that the system is successful in distinguishing condition, while the short time Fourier transform signal processing and deep residual network deep learning algorithm is superior to that of other models. The proposed framework and approach are scalable and generalizable and lay the foundation for the extension of the model.

Keywords: cyber-physical system; critical transmission components; smart production line; condition monitoring; machine learning



Citation: Song, L.; Wang, L.; Wu, J.; Liang, J.; Liu, Z. Integrating Physics and Data Driven Cyber-Physical System for Condition Monitoring of Critical Transmission Components in Smart Production Line. *Appl. Sci.* **2021**, *11*, 8967. <https://doi.org/10.3390/app11198967>

Academic Editor: José Machado

Received: 14 August 2021

Accepted: 21 September 2021

Published: 26 September 2021

Publisher's Note: MDPI stays neutral with regard to jurisdictional claims in published maps and institutional affiliations.



Copyright: © 2021 by the authors. Licensee MDPI, Basel, Switzerland. This article is an open access article distributed under the terms and conditions of the Creative Commons Attribution (CC BY) license (<https://creativecommons.org/licenses/by/4.0/>).

1. Introduction

Cyber–physical systems (CPSs) are an indispensable part of intelligent manufacturing (IM) and Industry 4.0, which is gradually transforming the landscape of the global manufacturing industry. CPSs are multidisciplinary systems that combine computation, communication, and control technologies to conduct real-time measurements, data transmission, monitoring, decision making, feedback control, and other functions on widely distributed embedded computing systems [1,2]. CPSs are considered to be a major feature of the new industrial revolution [3]. The deployment of a CPS system in Industry 4.0 has attracted the interest of many scholars and researchers [4]. Lee et al. [5] believe that the use of CPSs will move the manufacturing industry towards Industry 4.0; they proposed a unified 5C architecture as a guideline for deploying CPS. This guideline shows how to use the feedback from the initial data collection through to analytics in the final decision-making stage. Zhang et al. [6] presented a four-level unified architecture for a cyber–physical production system based on a digital twin. Liu et al. [7] presented a three-level CPS framework for workshops and introduced a guideline for the connection of physical components; obtaining and preprocessing data; visualizing results; and the

final knowledge acquisition. The various kinds of divisions of the CPS layer framework can be divided into five levels [2,3,5,8–13], four levels [6,14], and three levels [7,15], as shown in Table 1. These layers are divided into simple CPS workflows and basic concepts, the key CPS technologies and modeling methods used in the manufacturing field are not considered, and deep learning-based algorithms are not integrated in the framework.

Table 1. The division of CPS layers.

Number of CPS Framework Layers	Layer
five levels	[2,3,5,8–12]: 5C framework [13]: machine, data analysis, optimization, design layer
four levels	[6]: physical, network, virtual, application [14]: connection, features, mining and modeling, decision
three levels	[7]: physical connection, middleware, computation [15]: physical resources, local server, cloud server
Unclear delineated	[16–21]

Sophisticated machine learning (ML) based on industrial big data is a key component of CPSs that will enable us to reach a new phase of IM [22]. ML can extract the features of data collected by various sensors in a physical system and ultimately contribute to the integration of the physical system and cyber space. ML has been applied in practical industry and achieved impressive performance [23]. Shin et al. [8] proposed deploying a shop-floor CPS framework where a support vector machine was used as an ML technology for predicting the occurrence of anomalies. They designed and simulated this CPS framework based on ML for Industry 4.0. Ahmed et al. [3] proposed a real-time data-driven CPS with classification and regression ML algorithms implemented in the system. Wu et al. [21] proposed a novel ML algorithm for imbalanced data in a Prognostics and Health Management (PHM) CPS. Table 2 shows the application area and algorithm implementation of CPS. It can be seen from Tables 1 and 2 that the methods implemented by deep learning (DL) do not have a clear CPS architecture but simply involve the CPS field. Meanwhile, these methods only realize CPS applications based on data modeling, without considering the influence of physical modeling, and lack a framework to monitor the condition of critical transmission components (CTCs) in smart production lines (SPLs) from the perspective of CPS hybrid modeling.

Table 2. The application area and algorithm implementation of CPS.

CPS Application Area	CPS Algorithm Implementation
Workshop management system: [7,8] IM: [5,11–13] Biomedicine: [9,18] Welding: [2,3] PHM: [6,10,15,16,21] Production optimization: [17]	Shallow ML: [2,3,8–10] DL: [16,18–21]
Intelligent video monitoring system: [19] Transportation: [14] Object Detection: [20]	No algorithm implementation: [5–7,11–15,17]

With the development of IM and network collaborative manufacturing, data-driven SPL now plays an important role in ensuring the stable production of workshops, enterprises, and industrial chains [24–27]. The CTCs of SPL, such as motor spindles, bearings, and gears, operate under variable conditions for a long time. The breakdown of mechanical equipment in production lines is caused by motors, bearings, and gears, which account

for failure proportions of 27%, 41%, and 20%, respectively [28]. Xiao et al. [29] identified motors to be a vital component of the production line and showed that reliability analyses can ensure the reliable operation of the overall security of the SPL, enabling it to avoid economic losses and catastrophic accidents. Bampoula et al. [16] proposed a way to change from preventive maintenance to predictive in cyber–physical production systems and introduced a new DL model for estimating the remaining useful life (RUL) of the monitored equipment. A new automatic RUL prediction method for continuous production line equipment based on ML is proposed in [30]. Ayvaz et al. [31] developed a data-driven PHM for potential failures in production lines. Kang et al. [32] performed a systematic literature review of ML applications in production lines, where quality optimization, scheduling optimization, yield improvement, and product failure detection are the main research fields. DL technology has obtained significant achievements in SPL applications. There is great potential to realize the condition monitoring of CTC by integrating DL technology into a CPS architecture.

Within the background of network collaborative manufacturing, the integration of cyber and physical resources of SPL is further deepened and the condition monitoring of CTC has become a hot area in academia and industry. Some research gaps could be identified after reviewing the literature: (1) The research focuses on quality control, production scheduling, yield improvement, etc. The research on the condition monitoring of CTC in SPL is limited, especially that based on the data of motor spindles in the production line of machine tools. (2) There is a lack of a unified CPS framework and algorithm implementation that combines emerging technologies such as Internet of Things, big data, DL, etc., for CTC condition monitoring and reliability analysis in the manufacturing process of SPL. (3) The existing framework does not consider the key technical characteristics of CPS, especially those of deploying a CPS framework from the perspective of hybrid modeling.

In this paper, we proposed a theoretical CPS framework for CTC condition monitoring and reliability analysis, which is distinguished from existing solutions. Hybrid modeling, detailed algorithm implementation, and integrating DL rather than shallow ML are the main characteristics of the CPS framework. The accurate mapping of the vibration signal, which is easy to collect, and the CTC condition, which is difficult to obtain, was established. The effectiveness and predictive ability of the framework were validated with the use of multiple DL algorithms and signal processing steps through experiments on three datasets. The framework and approach proposed in this paper can be generalized to other SPL big data scenarios.

The structure of this paper is organized as follows. The deployment and implementation of the CPS framework and the description of the layers are presented in Section 2. The proposed hybrid model is elaborated on in Section 3. In Section 4, three experiments are carried out with different experimental results and the findings are provided to demonstrate the effectiveness of the developed CPS framework. Some observations and future directions are summarized in Section 5. Finally, conclusions are given in Section 6.

2. CPS Architecture for CTC Condition Monitoring

CPS is a computer-based technical system that has a clear architecture and sequential workflow manner that closely connects various complex processes and information from physical reality with that from cyber space, providing computation, communication, and control. Inspired by the layer architecture design of CPS, industrial big data, Internet of Things, and DL, this paper proposes a novel five-layer CPS framework which consists of the following layers: a smart connection layer, physics equation-based modeling (PEM) layer, ML-based modeling (MLM) layer, cognition layer, and configuration layer. The detailed architecture is shown in Figure 1, which presents the integration of physical components (e.g., motors, spindles, bearings, gears, and sensors) and cyber components (e.g., communication, computing, control).

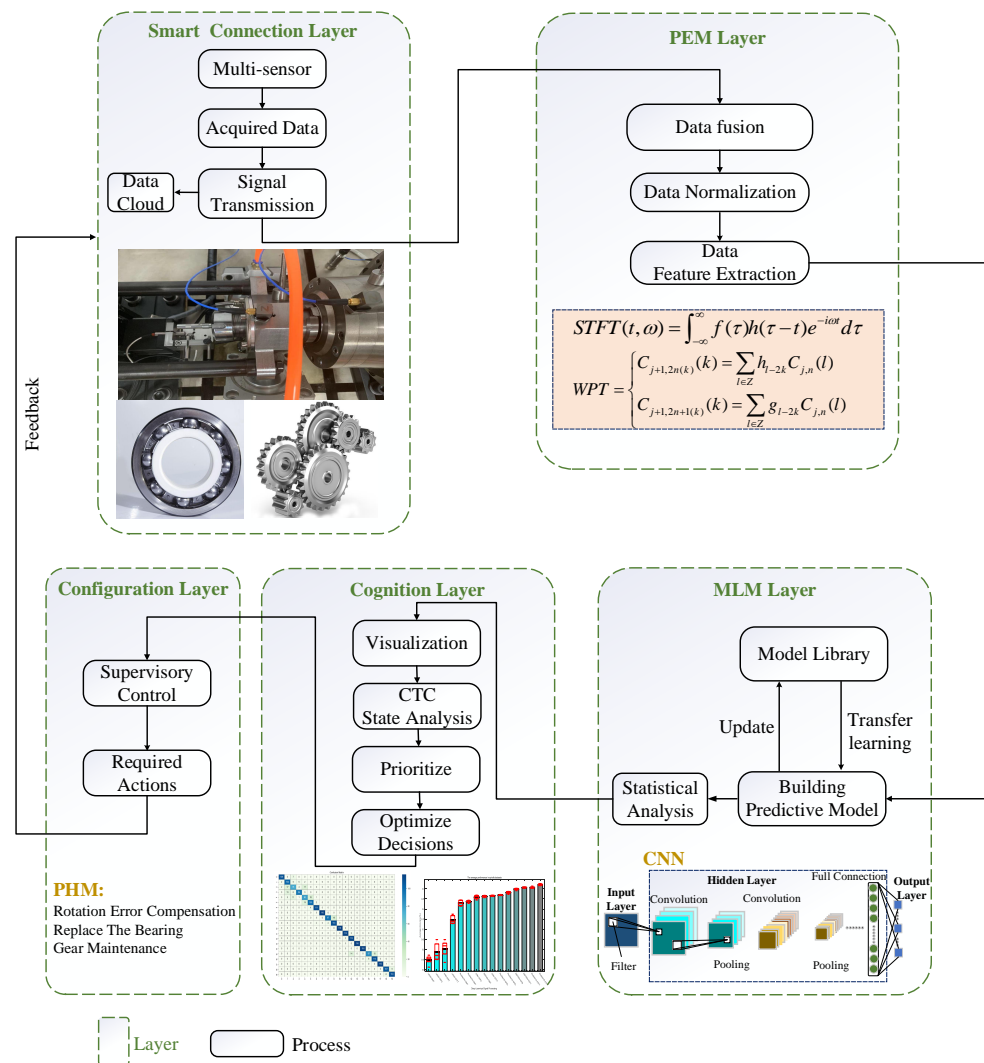


Figure 1. CPS framework for CTC condition monitoring and reliability analysis.

Smart Connection Layer: data acquisition is the main function of this layer. Sensors are the sensing elements of physical systems. Through reasonable multi-sensor position arrangement and type selection [33], variable accurate and reliable signals, such as vibration, current, force, and rotation error signals, can be collected. The collected datasets are transmitted to a large-capacity data storage device and saved in the cloud. Two important problems must be considered at this layer. Firstly, the type and specification of the sensor ensures the validity of the data, meaning whether the data are reliable. Secondly, the location of the sensor is related to the accuracy of the DL model, which relates to whether the data can be used to make accurate predictions.

PEM Layer: CPS modeling based on physical equations is the core technology used in this layer. The raw data are transferred to this layer through fieldbus and/or industrial Ethernet. Raw data are heterogeneous, imperfect, and large-scale [34] and cannot be directly used in the next layer. Data preprocessing, including data fusion, data normalization, and feature extraction, are the important considerations at this level. Through this layer, low-value data can be transformed into high-value information. The detailed physical modeling workflow will be discussed in Section 3.2.

MLM Layer: The meaningful information obtained from the PEM Layer is transferred to this level to build a CPS data-driven model, and a workflow from the physical components to the cyber components is established. This layer needs to provide support for the development of DL algorithms, the prediction model construction, and transfer learning and application implementation in a cyber virtual environment. Historical vibration data

will be used to develop and train the ML predictive model off-line, while real-time data are fed into the pretraining model to achieve online prediction. In practical applications, the problem of new datasets or tasks will be encountered; transfer learning can effectively solve this problem of models requiring training from scratch. The essence of this method is to solve new but similar tasks by applying knowledge that has been learned previously.

Cognition Layer: The real-time condition monitoring data of CTC and the prediction results from the MLM Layer can be displayed to experts through visualization techniques such as histograms and confusion matrices. In addition, the meaningful prediction results can be further analyzed and mined to evaluate the real-time equipment state. This layer informs us of the optimal decisions to be taken.

Configuration Layer: The core purpose of this layer is to transform the decision information of the cognition layer into maintenance activities and realize supervisory control from physical components to cyber components and back to physical components. The required PHM actions, such as rotation error compensation, replace the bearing, and gear maintenance, can be taken. The evaluation results of the CTC condition monitoring and reliability analysis enable a transition from preventive maintenance activities into predictive ones to be made.

3. Hybrid Modeling: Integrating Physics Preprocessing with Data-Driven Model

3.1. Physical and Data Driven Hybrid Model of CPS

There are two main modeling methods for CPS: modeling based on physical equations (PE) and modeling based on data. PE modeling uses underlying physics relationships to derive its mathematical representation; the main advantages of the PE model are its interpretability and scalability. Interpretability means that the PE model can better understand the modeling process from input to output, which is a white-box model. The causal relationship between parameters and variables is clear. Scalability is reflected in the complex CPS, which is composed of many physical subsystems. Any system of simple to moderate complexity can be established through the use of this method [35]. However, considering the complexity, uncertainty, and time-varying characteristics of CTC working conditions, the physical model is usually simplified [36] to a rough model that is an incomplete representation of the physical process of the real system. This process is time-consuming, expensive, and requires a high level domain expertise for industrial applications.

The ML method based on data eliminates the limitation of relying on system dynamics knowledge and completely depends on data, meaning that it is suitable for modeling different types of systems. However, as a complex mechanical system, the vibration signal of CTC usually contains a large amount of redundant information, and it is difficult to extract valuable state features without physical preprocessing. The use of appropriate data preprocessing will enable us to improve the prediction accuracy [37]. Therefore, the misuse of data and the DL model may lead to large errors or even obtain results that violate the laws of physics.

As shown in Figure 2, in order to fully utilize the advantages of PE and DL, a new hybrid CPS model based on physical preprocessing and data is proposed for CTC condition monitoring and reliability analysis. CPS modeling based on PE consists of three steps: raw vibration signal data fusion, data normalization, and feature extraction based on signal processing. Data fusion uses multi-sensor information, data normalization eliminates the influence of data distribution, and feature extraction can obtain valuable features from the original data. Input data X are transformed into \hat{X} after physical preprocessing. The high-value features of the previous step \hat{X} are divided into training sets and test sets and then sent into the DL model via CPS data modeling. Through model training and testing, the optimal DL model is used for the online deployment of SPL. The model training loss

Y_{ML} is calculated using the cross entropy loss function. The cross entropy loss function is expressed as:

$$Y_{ML} = - \sum_{i=1}^N p_i(x) \log(q_i(x)) \tag{1}$$

where N is the number of the classes, $q_i(x)$ denotes predictive probability of the input data X belonging to i th class, $p_i(x)$ denotes real probability.

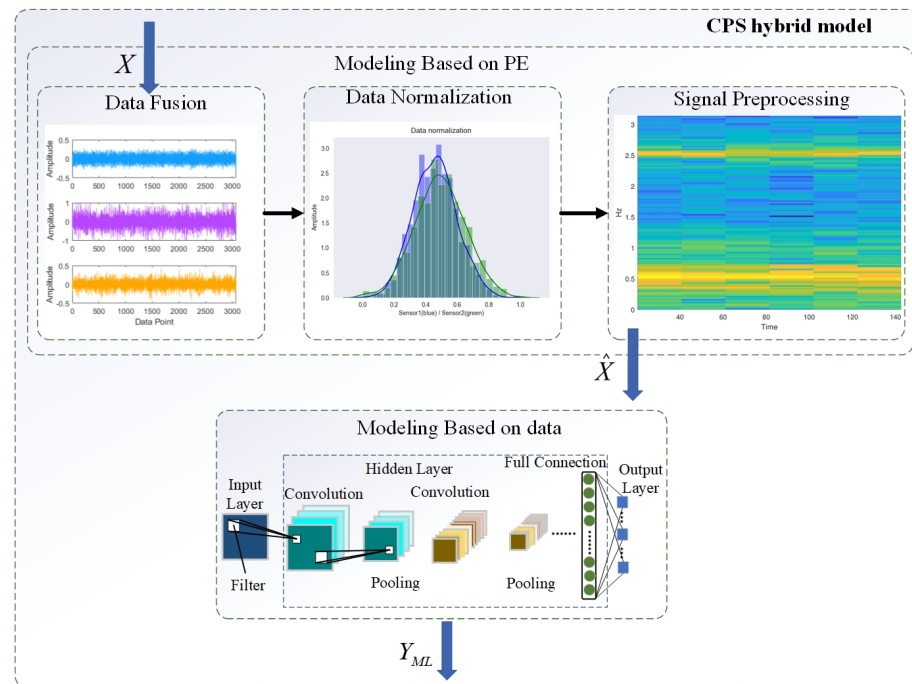


Figure 2. A detailed flow chart of CPS hybrid modeling.

3.2. CPS Modeling Based on PE

Multi-sensor data fusion, as shown in Figure 2, can merge data to make them more informative. The data collected by CPSs are multi-source and heterogeneous. Normalization is therefore necessary in order to eliminate the limitations of data units and make them dimensionless, which is convenient for the comparison and weighting of different units or scales. Meanwhile, data normalization can accelerate the convergence of DL models [38]. As shown in Figure 2, the data distribution range of sensor 1 and sensor 2 is made more consistent through the use of data normalization. The normalization method is expressed as:

$$X^* = \frac{X - Min}{Max - Min} \tag{2}$$

where X represents the input sample, Max is the maximum value of the sample data, Min is the minimum value of the sample data, and X^* is the normalized output.

In order to extract the meaningful state features from the data and reduce the difficulty of DL training, it is necessary to perform signal processing, which is realized by the PE modeling of the raw data. This processing method can enable us to meet the requirements of 2D convolutional neural networks (CNNs) for two-dimensional matrix inputs. Short-time Fourier transform (STFT) and wavelet packet decomposition (WPD) are able to extract the time–frequency characteristics of data. In addition, this paper also evaluates the accuracy of data matrix transformation (DMT) without signal processing.

STFT: As shown in Figure 3a, through the spectrum function of MATLAB, a section of the time sequence signal can be directly transformed into a time–frequency heat map through STFT. The horizontal axis represents time and the vertical axis represents frequency, while different colors represent different values. The theory of STFT is to multiply the

original signal by the window function and carry out the segment-by-segment Fourier transform of the original signal by moving the window function. The window functions commonly used by STFT include rectangular, Hanning, and Gaussian. The equation of STFT is expressed as:

$$\text{STFT}(t, \omega) = \int_{-\infty}^{+\infty} f(\tau)h(\tau - t)e^{-j\omega t}d\tau \tag{3}$$

where t and τ denote the time, ω denotes the frequency, $f(t)$ is the time-domain data, $h(\tau - t)$ is a window function whose center is at time t , and $\text{STFT}(t, \omega)$ is the time–frequency matrix after STFT. Supposing that the length of a signal sample is 1024, through a Hanning window STFT with the length of 64, the output data are a 33×33 time–frequency matrix.

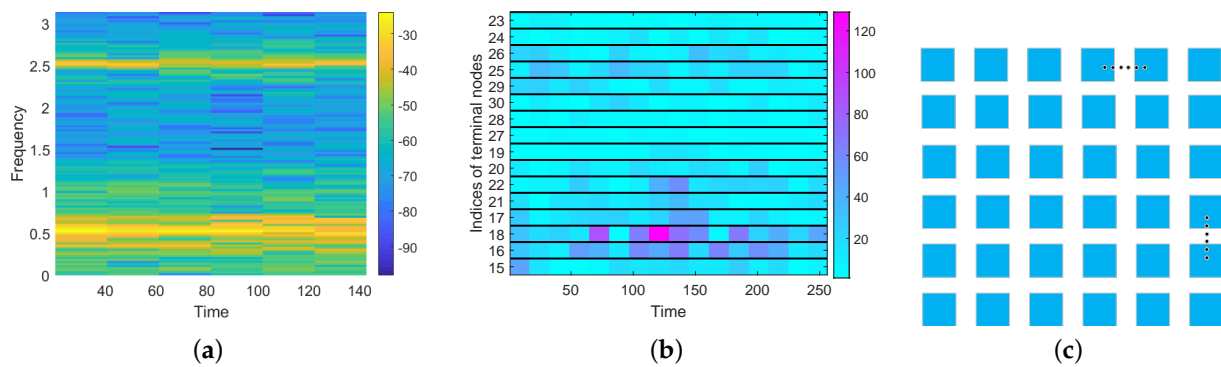


Figure 3. Signal preprocessing based on PE. (a) STFT. (b) WPD. (c) DMT.

WPD: As illustrated by Figure 3b, WPD can decompose each vibration signal sample into a sub-band containing a series of wavelet coefficients through the `wpdec` function of MATLAB. WPD’s heatmap horizontal axis represents time, the vertical axis represents different sub-bands, and different colors represent different values. WPD is a widely used time–frequency analysis method. The equation of WPD is expressed as:

$$\begin{cases} C_{j+1,2n}(k) = \sum_{l \in \mathbb{Z}} h_{l-2k}C_{j,n}(l) \\ C_{j+1,2n+1}(k) = \sum_{l \in \mathbb{Z}} g_{l-2k}C_{j,n}(l) \end{cases} \tag{4}$$

where j and n represent the number of WPD layers and sub-bands, respectively; $C_{j,n}$ denotes the wavelet coefficient sequence of the n th node in the j th layer; $C_{0,0}$ is the original signal; and h and g denote the high-pass filter and low-pass filter, respectively. The equation between h and g is given as:

$$g(k) = (-1)^k h(k) \tag{5}$$

In this paper, DB25 is used as the wavelet basis function and a signal length of 1024 is transformed into a 64×64 wavelet coefficient matrix through 6-level WPD. A brief illustration of WPD is shown in Figure 4. The wavelet coefficients of different subbands can be obtained by multi-level WPD.

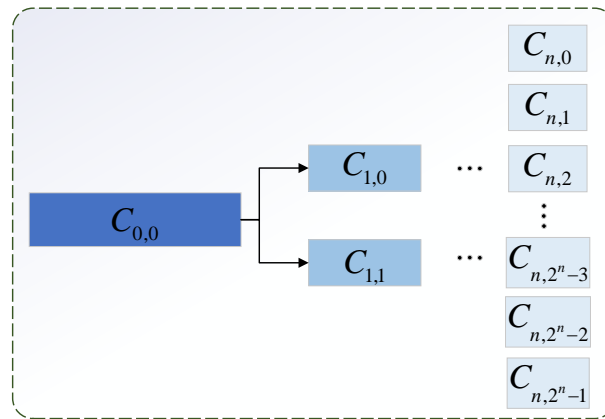


Figure 4. A brief illustration of WPD.

DMT: The raw data are reshaped from a one-dimensional time sequence signal to a two-dimensional signal without signal processing. A simple illustration of DMT is shown in Figure 5, numbers 0 to 1023 denote time sequence signal data point, and each blue square represents the value of the matrix. Supposing that the length of a signal sample is 1024, through DMT, the output data are made into a 32×32 matrix.

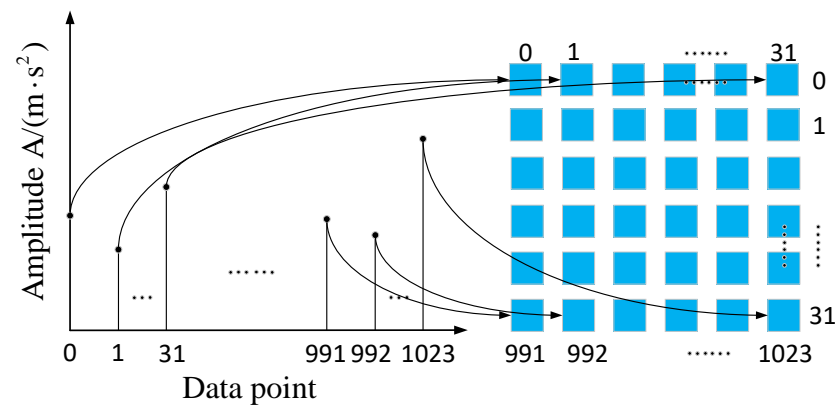


Figure 5. A brief illustration of DMT.

3.3. CPS Modeling Based on DL

As the most important branch of ML, DL has been widely used in computer vision [39,40] and natural language processing [41,42]. We tested the performance of four categories of representative models that are based on CNN, including 5-layer CNN, LeNet, multi-scale CNN (MSCNN), and residual networks (ResNet).

CNN has great advantages in processing matrix data. Sparse connections and weight sharing are its main characteristics. As shown in Figures 6 and 7, CNNs generally include five parts: an input layer, convolution layer, pooling layer, full connection layer, and output layer. BN is batch normalization, ReLU is rectifier linear unit activation function, Conv is convolution layer, GAP is global average pooling layer, MP is max pooling layer, AMP denotes adaptive max pooling layer, green cubes with different shades of color represent convolution operations with different convolution kernel sizes. LeNet is a CNN structure with a small number of channels which was first applied for image recognition [43]. Wu et al. [44] applied LeNet for bearing fault diagnosis. A 5-layer CNN is a medium-sized CNN structure with a final output channel size of 128 [38]. The size of the convolution kernel is vital in CNN, as different convolution kernel sizes can extract features of different scales. The design idea of MSCNN comes from the novel network structure inception [45], which can extract multi-scale features through parallel convolution branches. The MSCNN contains three scales, and each scale consists of different kernel sizes, meaning that various global features and local features of the time–frequency matrix can be extracted. Finally,

the extracted features are concatenated together for classification. The combination of local and global feature extraction used for MSCNN has been used in gearbox condition monitoring [46] and bearing fault diagnosis [47]. In CNN, as the number of network layers increases, the phenomena of gradient disappearance and gradient explosion will occur, which makes it difficult to train the network. Deep ResNet, as shown in Figure 7, is an improved variant of CNN that uses identity shortcuts to ease the difficulty of training [48]. ResNet include a series of residual building units (RBU); an RBU can be composed of BN, ReLU, and Conv. The output of each RBU is expressed as:

$$Y = F(X) + X \tag{6}$$

where X denotes the input of RBU, $F(X)$ denotes the output of convolution operation, and Y represents the output of RBU.

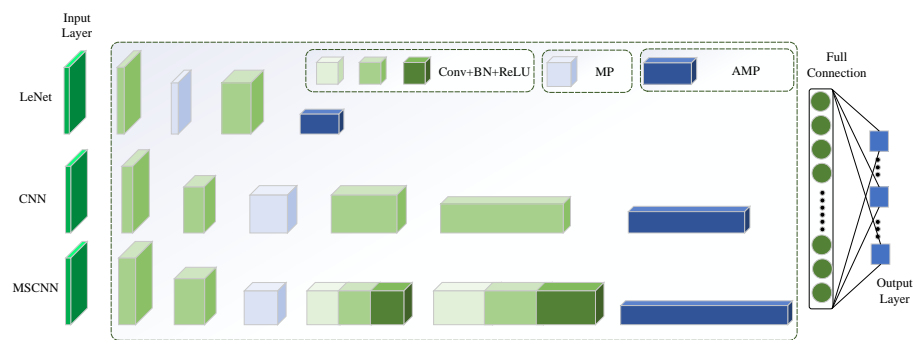


Figure 6. A brief architecture of LeNet, CNN, and MSCNN.

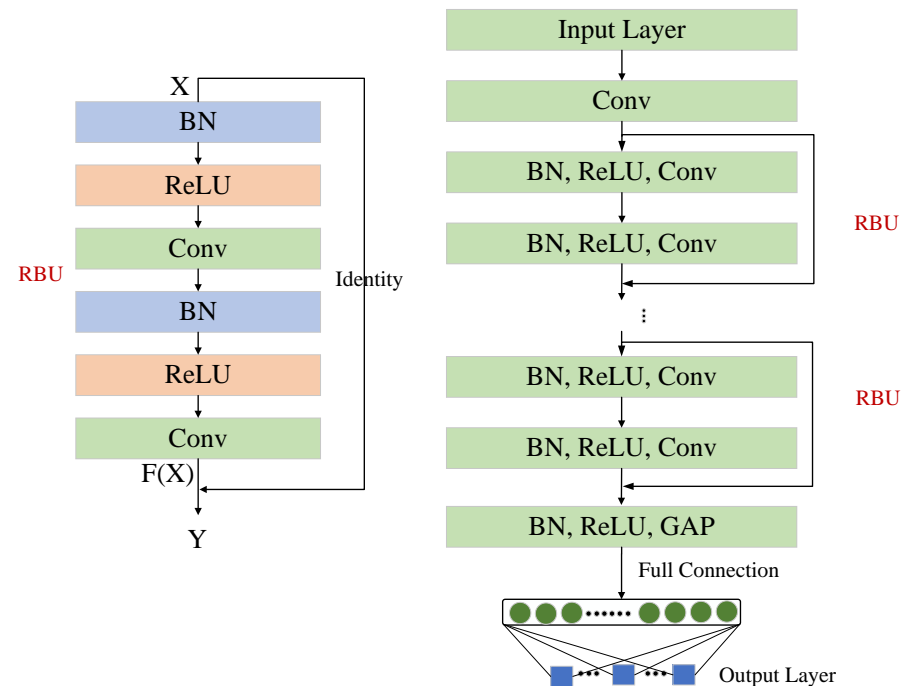


Figure 7. A brief architecture of ResNet.

Considering the WPD input as an example, the detailed structure and feature size of each layer are shown in Table 3, where 3×3 , 5×5 , and 7×7 denote Conv+BN+ReLU with kernel sizes of 3, 5, and 7; and $\times 2$ means that the same RBU block is appended two times in sequence. The output sizes of each layer, such as 8, 62, 62 are the number of channels, the height, and the width. In the spindle datasets, the first MP was removed.

Table 3. Feature size output by each layer of the DL algorithm.

CNN	LeNet	MSCNN	ResNet10	ResNet18
$\begin{bmatrix} 3 \times 3 \\ 8, 62, 62 \end{bmatrix}$	$\begin{bmatrix} 5 \times 5 \\ 6, 60, 60 \end{bmatrix}$	$\begin{bmatrix} 3 \times 3 \\ 16, 62, 62 \end{bmatrix}$	$\begin{bmatrix} 7 \times 7 \\ 64, 32, 32 \end{bmatrix}$	$\begin{bmatrix} 7 \times 7 \\ 64, 32, 32 \end{bmatrix}$
$\begin{bmatrix} 3 \times 3 \\ 16, 60, 60 \end{bmatrix}$	$\begin{bmatrix} \text{MP} \\ 6, 60, 60 \end{bmatrix}$	$\begin{bmatrix} 3 \times 3 \\ 32, 60, 60 \end{bmatrix}$	$\begin{bmatrix} \text{MP} \\ 64, 16, 16 \end{bmatrix}$	$\begin{bmatrix} \text{MP} \\ 64, 16, 16 \end{bmatrix}$
$\begin{bmatrix} 3 \times 3 \\ 32, 58, 58 \end{bmatrix}$	$\begin{bmatrix} 5 \times 5 \\ 64, 26, 26 \end{bmatrix}$	$\begin{bmatrix} \text{MP} \\ 32, 30, 30 \end{bmatrix}$	$\begin{bmatrix} \text{RBU}, 3 \times 3 \\ 64, 16, 16 \end{bmatrix} \times 1$	$\begin{bmatrix} \text{RBU}, 3 \times 3 \\ 64, 16, 16 \end{bmatrix} \times 2$
$\begin{bmatrix} \text{MP} \\ 32, 29, 29 \end{bmatrix}$	–	$\begin{bmatrix} 3 \times 3, 5 \times 5, 7 \times 7 \\ 192, 30, 30 \end{bmatrix}$	$\begin{bmatrix} \text{RBU}, 3 \times 3 \\ 128, 16, 16 \end{bmatrix} \times 1$	$\begin{bmatrix} \text{RBU}, 3 \times 3 \\ 128, 16, 16 \end{bmatrix} \times 2$
$\begin{bmatrix} 3 \times 3 \\ 64, 27, 27 \end{bmatrix}$	–	$\begin{bmatrix} 3 \times 3, 5 \times 5, 7 \times 7 \\ 768, 30, 30 \end{bmatrix}$	$\begin{bmatrix} \text{RBU}, 3 \times 3 \\ 256, 16, 16 \end{bmatrix} \times 1$	$\begin{bmatrix} \text{RBU}, 3 \times 3 \\ 256, 16, 16 \end{bmatrix} \times 2$
$\begin{bmatrix} 3 \times 3 \\ 128, 25, 25 \end{bmatrix}$	–	–	$\begin{bmatrix} \text{RBU}, 3 \times 3 \\ 512, 16, 16 \end{bmatrix} \times 1$	$\begin{bmatrix} \text{RBU}, 3 \times 3 \\ 512, 16, 16 \end{bmatrix} \times 2$
$\begin{bmatrix} \text{AMP} \\ 128, 6, 6 \end{bmatrix}$	$\begin{bmatrix} \text{AMP} \\ 128, 5, 5 \end{bmatrix}$	$\begin{bmatrix} \text{AMP} \\ 768, 4, 4 \end{bmatrix}$	$\begin{bmatrix} \text{GAP} \\ 512, 1, 1 \end{bmatrix}$	$\begin{bmatrix} \text{GAP} \\ 512, 1, 1 \end{bmatrix}$

4. CPS Framework Implementation and Experimentation

Spindle motors, bearings, and gears are three CTCs of SPL equipment. Component failure will seriously affect the normal operation of the SPL and cause huge economic losses [29,49–51]. Therefore, in this paper, the prediction of spindle motor rotation error and the fault diagnosis of bearings and gears based on two public datasets are used to verify the ability of the proposed CPS framework to tackle the condition monitoring problems of SPL.

4.1. Case 1: The Prediction of Spindle Motor Rotation Error

As complex systems integrating mechanical, electrical, hydraulic, and pneumatic aspects, spindle motors are the CTC of SPL. The rotation error of a spindle is closely related to the geometric error, surface quality, and roughness of the workpiece, which is an important index used to reflect the reliability of machine tools [52,53]. Therefore, the accurate prediction of spindle rotation error is of great significance for improving machining precision and efficiency. The existing rotation error measurement methods are usually implemented with the aid of a standard ball in the case of idle conditions [54–56], which makes it difficult to reflect the real error in the actual machining process. The derivation of the method used for predicting the rotation error based on the physical dynamics model is complicated and inaccurate [36,57]. It is difficult to achieve real-time condition monitoring and real-time rotation error compensation. The spindle rotation error can be affected by the speed [55] and wear state [36,57]. Fortunately, the spindle vibration data contain information related to the speed [58] and wear state [59]. Therefore, it is possible to predict the rotation error through vibration data.

As shown in Figure 8, the spindle reliability experiment platform of Tsinghua University was established based on CPS. A loading experiment was carried out through the spindle load spectrum [60] to ensure that the spindle load was close to the actual machining. The spindle rotation error was collected by the spindle check machine capability tester every 10 h, and the wear test was carried out during the rest time.

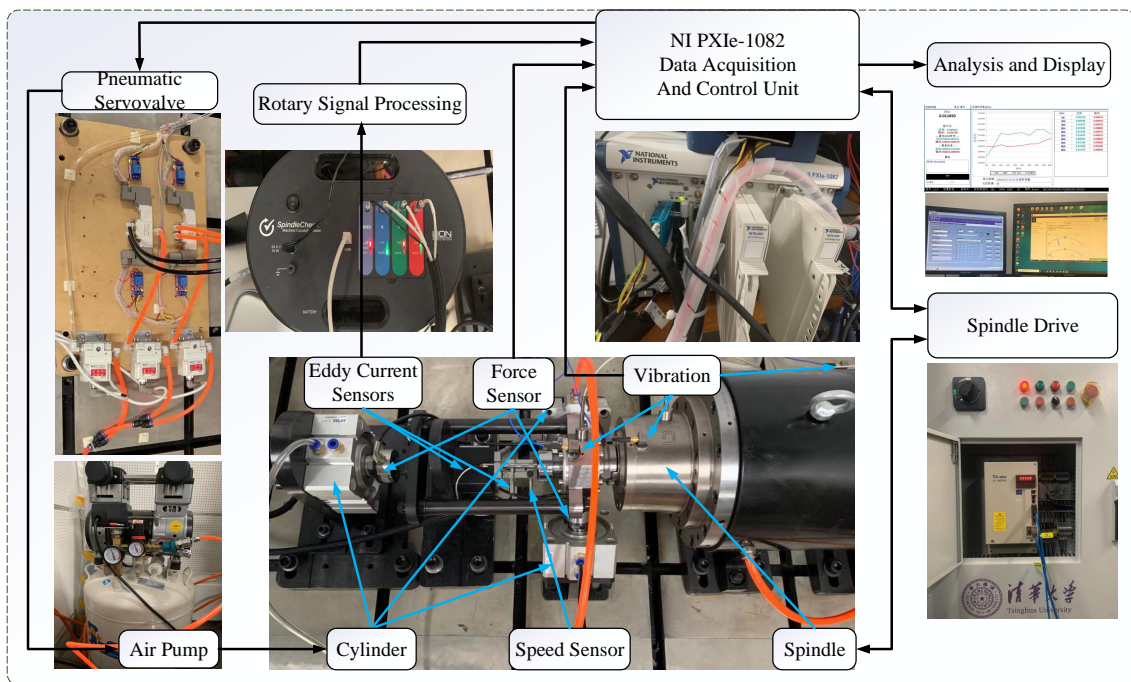


Figure 8. The spindle experimental platform.

Sensors: The vibration sensors were installed on the base, bearing, and spindle to collect vibration signals. The force sensor collected the load force to realize the closed-loop control of the load spectrum; the speed sensor measured the spindle speed to realize closed-loop control; and the eddy current sensor was used to detect the spindle displacement. The rotation error could be obtained by a spindle check machine capability tester. A detailed description of the smart connection layer components is provided in Table 4, including the key components of the smart connection layer: specification, communication mode, and function. These constitute the smart connection layer of CPS.

Table 4. Detailed description of the Smart Connection Layer components.

Key Components of Smart Connection Layer	Specification	Communication Mode and Function
Spindle and spindle drive	CTB40D	PXIe-1082 communicates with spindle driver through RS485-USB interface to control spindle torque, acceleration and deceleration
Vibration sensor	PCB 256A14	Connect with PXIe-1082 through Integrated Electronic Piezo-Electric interface to collect vibration signals
Force sensor	DYMH-104	The 4-line difference signal is fed back to the analog input channel of PXIe-1082
Spindle check machine capability tester	Lion	The output digital signal of the tester is directly connected with the NI PXIe-1082 through the USB interface, three eddy current sensors and one speed sensor are integrated in the tester
Data acquisition and control unit	NI PXIe-1082	Data acquisition and spindle control
Pneumatic loading unit	AirTac-100	PXIe-1082 controls the pneumatic loading unit through analog output channel

PXIe-1082: A data acquisition and control unit is the core component of the system and is mainly used to realize the loading control of air pump, multi-sensor data acquisition, data transmission to the analysis platform, spindle drive, and feedback control. The configuration layer of the CPS is realized in this part.

Data analysis platform: This part is based on MATLAB and Python. The acquisition and control unit sends the data to the analysis platform to support the PEM layer, MLM layer, and cognition layer of CPS, which is the core part of the data processing and rotation error prediction.

After the data acquisition, it is necessary to preprocess the vibration signal and the corresponding rotation error. The spindle speed ranges from 1000 r/min to 4000 r/min; the experiment shows that the variation range of rotation error is 5–14.5 μm . After discretization, the rotation error data are rounded to the nearest 0.5. Therefore, there are 20 types of rotation error and the number class is set to 20. Two datasets of each class for a total of 40 datasets were selected for the experiment; each dataset contained $200,000 \times 3$ ($\times 3$ means 3 sensors) raw data points. The former 70% of data points were selected as the training data, while the last 30% were used as testing data. In this paper, the sample length was 1024 data points and the shift length [61] was 320 data points. Hence, the total number of samples in each class was 870 and the total number of training samples was 20×870 . Data augmentation was not used in the testing set, and the total number of testing samples was 20×116 .

4.2. Case 2: The Fault Diagnosis of Bearing

The bearing datasets contained 12 vibration sub-datasets, and the number class was 12. Vibration signals were collected at the three speeds of 600 r/min, 800 r/min, and 1000 r/min. Each working condition contained one normal state and three fault modes, which include rolling elements, outer rings, and inner rings. Detailed descriptions of the bearing datasets are shown in Table 5. The detailed description of the experimental platform can be found in reference [62]. After data preprocessing, the total number of training samples was 7038 and the total number of testing samples was 1764.

Table 5. Detailed description of the bearing datasets.

Fault Mode	Speed (r/min)
rolling element	600, 800, 1000
outer ring	600, 800, 1000
inner ring	600, 800, 1000
normal state	600, 800, 1000

4.3. Case 3: The Fault Diagnosis of Gear

The gear datasets contained 20 vibration sub datasets and the number class was 20. Vibration signals were collected in two kinds of working conditions. Each working condition contained two normal states and eight fault modes. Detailed information on the gear datasets is displayed in Table 6. A detailed description of the experimental platform can be found in the reference [63]. In particular, for this gear drivetrain diagnostics simulator datasets, Gaussian noise with a signal-to-noise ratio of 1 dB is added to the vibration signal [64]. After data preprocessing, the total number of training samples was 16,380 and the total number of testing samples was 4100.

Table 6. Detailed description of the gear datasets.

Fault Mode	Working Condition
normal gear	20 Hz—0 V, 30 Hz—2 V
normal bearing	20 Hz—0 V, 30 Hz—2 V
chipped tooth	20 Hz—0 V, 30 Hz—2 V
missing tooth	20 Hz—0 V, 30 Hz—2 V
root	20 Hz—0 V, 30 Hz—2 V
surface	20 Hz—0 V, 30 Hz—2 V
inner ring	20 Hz—0 V, 30 Hz—2 V
outer ring	20 Hz—0 V, 30 Hz—2 V
inner+outer ring	20 Hz—0 V, 30 Hz—2 V
rolling element	20 Hz—0 V, 30 Hz—2 V

4.4. Experiment and Result Analysis

This part focuses on the performance of different DL methods rather than the setting of the hyperparameters. In the experiment, different methods in the same datasets used the same hyperparameters. The learning rate was 0.001 for spindle datasets. The learning rate was 0.001 from 0 to 29 epochs, 0.0001 from 30 to 59 epochs, and 0.00001 in the last 40 epochs for the bearing and gear datasets. The mini-batch size was 64 and the maximum number of epochs was 100. In the process of model training, Adam was used as the optimizer. Momentum is an important parameter of Adam and can accelerate the training process; it was set to 0.9 following the setup seen in [65].

The experiments were conducted on a system with i7 CPU @3.80 GHz and NVIDIA GeForce RTX 2060 SUPER. Python was used as a programming environment with pytorch. In the experiment, the maximum accuracy across all the epochs was chosen as the testing accuracy. In this experiment, we evaluated the accuracy when using different signal processing procedures and DL algorithms. In order to reduce the impact of the randomness, five trials were carried out for each experiment. The average performance of these methods, including LeNet, CNN, MSCNN, ResNet10, ResNet18, long short-time memory network (LSTM), and bidirectional LSTM (BiLSTM) [40], are shown in Tables 7–9 and Figures 9–11, in which the horizontal axis represents the combination of different DL algorithms and signal processing, the vertical axis represents the average accuracy, the histogram and black numbers represent the average accuracy value and the red box chart shows the dispersion at five times. STFT and ResNet obtained the best accuracy values of 92.08%, 95.12%, and 94.56%, respectively, in all three datasets.

Table 7. Experimental results of the spindle datasets.

Signal Processing	Average Testing Accuracy \pm Standard Deviation (%)						
	MSCNN	CNN	LeNet	ResNet10	ResNet18	LSTM	BiLSTM
DMT	82.96 \pm 1.39	74.78 \pm 2.10	54.95 \pm 2.21	58.87 \pm 4.41	60.43 \pm 4.31	61.66 \pm 1.55	62.20 \pm 0.80
STFT	90.65 \pm 0.26	85.90 \pm 0.98	86.88 \pm 0.21	90.69 \pm 0.39	92.08 \pm 0.41	88.90 \pm 0.64	89.77 \pm 0.28
WPD	89.88 \pm 0.47	88.21 \pm 0.54	83.73 \pm 0.55	86.59 \pm 0.23	86.28 \pm 0.43	84.41 \pm 0.45	84.85 \pm 1.04

Table 8. Experimental results of the bearing datasets.

Signal Processing	Average Testing Accuracy \pm Standard Deviation (%)						
	MSCNN	CNN	LeNet	ResNet10	ResNet18	LSTM	BiLSTM
DMT	89.05 \pm 0.80	82.69 \pm 1.34	59.15 \pm 1.48	86.63 \pm 0.61	86.03 \pm 0.66	80.41 \pm 0.68	80.40 \pm 0.90
STFT	93.48 \pm 0.27	90.41 \pm 1.14	83.87 \pm 1.37	95.02 \pm 0.22	95.12 \pm 0.20	89.90 \pm 0.79	91.01 \pm 0.56
WPD	91.94 \pm 0.53	88.53 \pm 0.91	70.58 \pm 1.64	91.15 \pm 0.40	91.10 \pm 0.46	83.80 \pm 0.73	84.79 \pm 0.63

Table 9. Experimental results of the gear datasets.

Signal Processing	Average Testing Accuracy ± Standard Deviation (%)						
	MSCNN	CNN	LeNet	ResNet10	ResNet18	LSTM	BiLSTM
DMT	94.06 ± 0.46	88.45 ± 0.19	64.80 ± 4.42	93.66 ± 0.37	93.08 ± 0.51	77.95 ± 1.20	77.24 ± 0.25
STFT	94.41 ± 0.23	91.77 ± 0.82	88.24 ± 0.35	94.56 ± 0.27	93.98 ± 0.15	92.24 ± 0.37	92.55 ± 0.42
WPD	83.97 ± 1.88	86.27 ± 1.54	74.18 ± 2.18	90.50 ± 0.61	89.53 ± 0.43	83.69 ± 0.80	84.13 ± 0.40

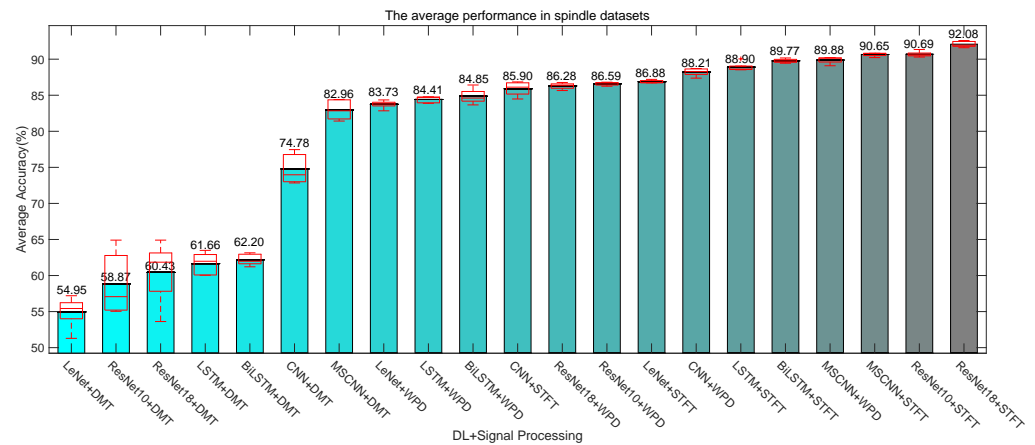


Figure 9. The results of the spindle datasets.

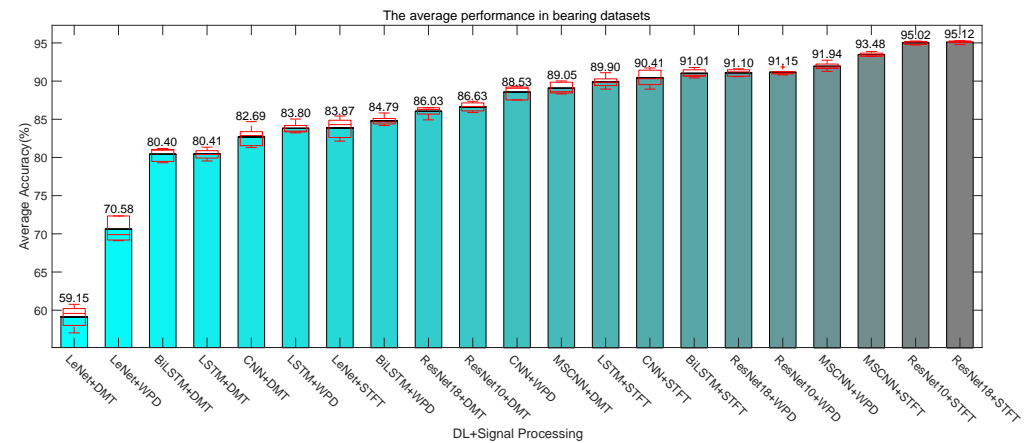


Figure 10. The results of the bearing datasets.

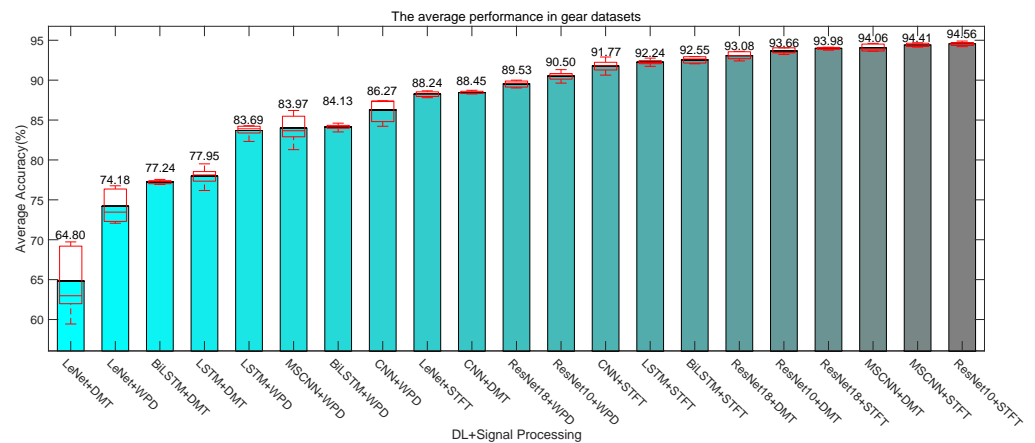


Figure 11. The results of the gear datasets.

As can be seen from Tables 7–9 and Figures 9–11, STFT always obtains the best accuracy in three datasets, the overall average accuracy is STFT > WPD > DMT. STFT and WPD can be used to gain the time–frequency characteristics of the data, and their accuracy is significantly higher than that of DMT. This result proves the necessity of the proposed PEM layer. The reason why the accuracy of STFT is higher than that of WPD is that the matter of how to choose the optimal wavelet basis function and wavelet decomposition level is challenging. For example, in the experiment, it was found that the accuracy of the CNN in spindle datasets was 72.24% for five-level wavelet decomposition under a DB1 wavelet basis function and 88.21% for six-level wavelet decomposition under a DB25 wavelet basis function, which represents an improvement of 15.97%.

At the same time, we can see that the ResNet can always obtain the best accuracy. The order for the accuracy of the proposed hybrid modeling in three datasets with STFT is ResNet > MSCNN > BiLSTM > CNN > LeNet. Compared with other methods, the accuracy of LeNet is the lowest. As the depth of LeNet is the shallowest and the number of convolution channels here is the lowest, the features contained in the signal cannot be extracted completely. CNN has more channels than LeNet and can extract more feature information, so the accuracy of CNN is greater than LeNet. The BiLSTM designed in reference [38] can not only extract spatial feature information through convolution, but also extract temporal information. The accuracy of BiLSTM is greater than CNN. BiLSTM can extract bidirectional temporal features, and its accuracy is greater than LSTM. MSCNN can extract multi-scale features, which significantly improves the feature extraction ability, and the performance of MSCNN is better than that of BiLSTM, CNN and LeNet. With the network depth increases, ResNet can overcome the phenomena of gradient disappearance and explosion, which makes the network easy to train; thus, ResNet has the best accuracy. In the spindle and bearing datasets, ResNet18 performs better than ResNet10. In gear datasets, ResNet10 performs better than ResNet18. This may be due to the slight overfitting of the gear datasets.

Through the above analysis, the method proposed in this paper successfully monitors the condition of CTC in SPL. The experimental results of STFT, WPD, DMT and different DL algorithms show the necessity of CPS hybrid modeling and the feasibility of algorithm implementation.

To better understand the classification effect of these models for each label, Figure 12 shows the confusion matrices of LeNet, CNN, LSTM, BiLSTM, MSCNN, and ResNet18 in bearing datasets with STFT signal processing. In Figure 12, it is evident that almost all the categories in the ResNet18 model are easier to diagnose than those of other models, except for label 4, where ResNet18 is slightly less easy to diagnose than MSCNN.

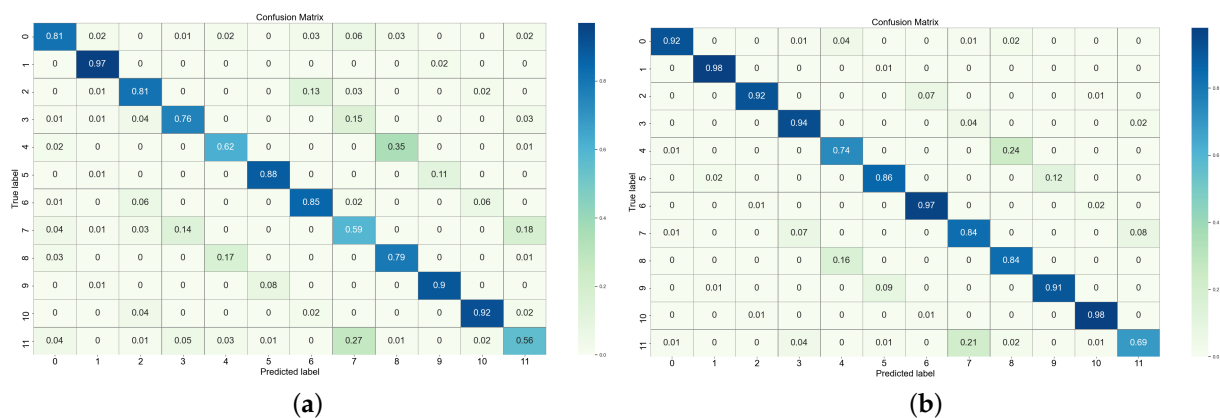


Figure 12. Cont.

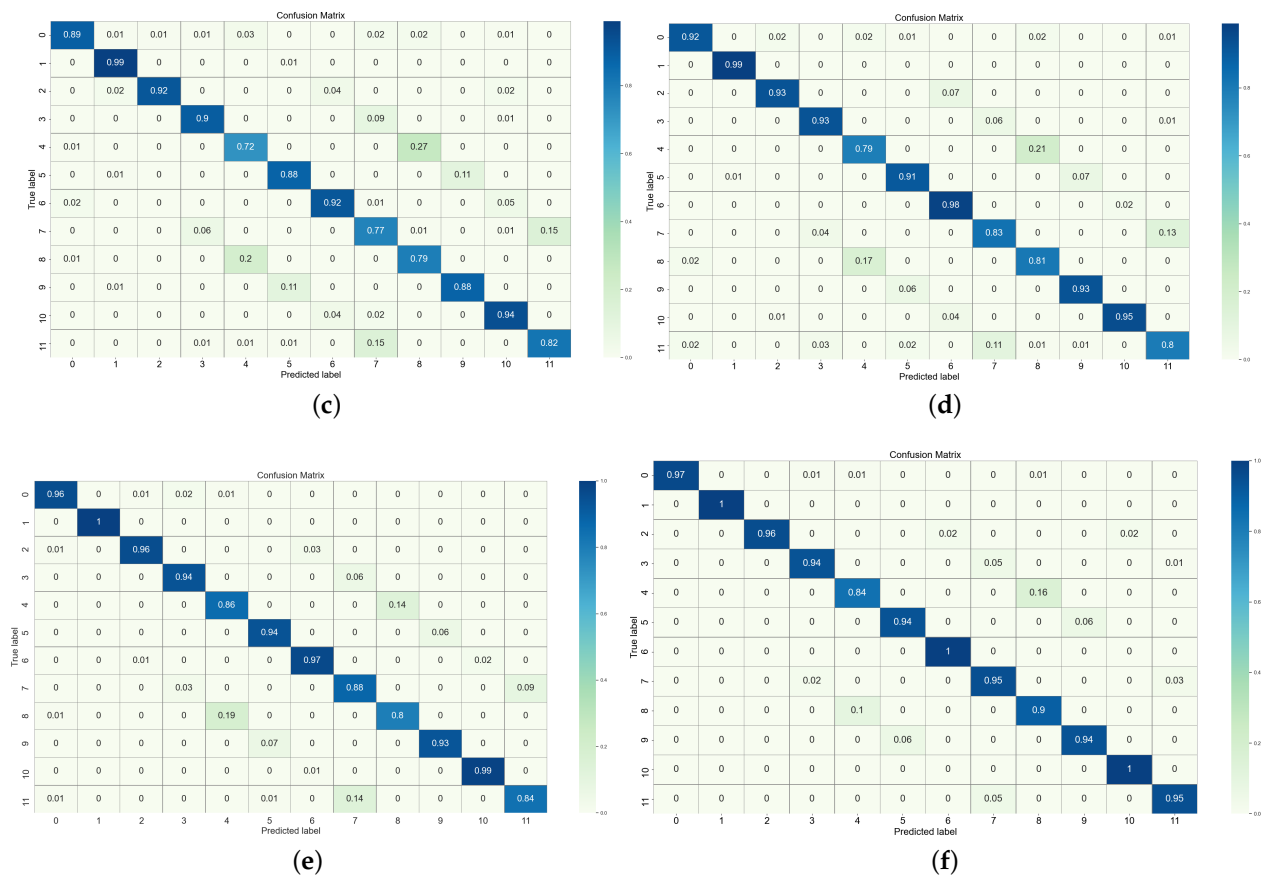


Figure 12. Confusion matrix of bearing datasets. (a) LeNet. (b) CNN. (c) LSTM. (d) BiLSTM. (e) MSCNN. (f) ResNet18.

5. Discussions and Future Works

(1) Modeling Based on PE

Vibration data have the characteristics of high dimensionality, nonlinearity, and diversity. Signal processing is the core of the PEM layer. Other signal processing methods, including empirical mode decomposition, local mean decomposition, and Hilbert–Huang transform, can extract discriminative features from different domains, and those feature extraction methods are worth studying. In the PEM layer, the question of how to extract valuable features from noisy data and extract a sufficient number of features from imbalanced data are two problems that need to be considered. CTC often operates under harsh working environments, and the vibration signal collected often contains irregular noise. Feature information can easily be annihilated by strong background noise. At the same time, it was found that the distribution between each category of samples was imbalanced in our experiment. In the context of CPS hybrid modeling, there is still a great amount of progress to be made in the feature extraction of noisy and imbalanced data.

(2) Modeling Based on data

Whether the data-driven CPS framework can be successfully deployed in the SPL depends on the quality of the datasets used. The more labeled multi-sensor data are available, the better the accuracy will be. In fact, the use of data with less labels limits the application of DL in the CPS. The other problem is represented by limited data. A major challenge in this CPS framework is in obtaining a sufficient amount of training data, which is a time-consuming, laborious, and costly process. The use of semi-supervised or unsupervised DL for less-labeled data and few-shot learning with a meta-learning paradigm for limited data are techniques that have been widely used in the field of computer vision. These methods are worth using in attempts to solve the above problems.

(3) Integrating digital twin with CPS

CPS improves the communication between physical and cyber space. In a digital twin, a high-fidelity digital copy is built through big data and physical models in physical systems to provide services for CPS monitoring, analysis, decision making, and feedback to physical entities. The question of how to integrate digital twins with CPS for the condition monitoring of CTC in SPL would be an interesting research direction to explore in the future.

(4) Infusing 5G into CPS

Various industrial Ethernet and fieldbus technologies are still the main data transmission technologies used in CPSs. Some wireless transmission technologies, such as Bluetooth and ZigBe, etc., have also been applied to CPS. 5G promotes the development of wireless communication technology. Its main features are enhanced mobile broadband, low latency, high reliability, and mass machine communication. 5G can effectively meet the needs of CPS for large-scale data acquisition and sensing, precise control, remote processing. The question of how to deploy 5G in all layers of CPS, especially in the smart connection layer, should be addressed in future research.

6. Conclusions

In this paper, CPS hybrid modeling was investigated and a novel five-layer architecture which included a PEM layer and an MLM layer was proposed for CTC condition monitoring in SPL. The CPS framework integrated various DL-based algorithms. Firstly, the multi-sensor data of the SPL monitoring CTC were collected via a smart connection layer; then, a large amount of low-value data was transformed into high-value feature information through the PEM layer. After this, the feature information was used to train and evaluate the DL model through the MLM layer; visualization techniques helped us to make more effective and scientific decisions via the cognition layer. Finally, the decision information was transformed into predictive maintenance activities through a configuration layer. Therefore, the CPS framework was able to realize a closed-loop workflow and reduce the potential for failures that could impact SPL operations. The effectiveness and predictive power of the developed CPS framework, hybrid modeling, and algorithm implementation were verified by the DL and signal processing methods. The proposed framework and approach could be generalized in order to predict the RUL, product quality, etc. from scratch with the integration of additional sensors and a training DL model, which would lay the foundation for framework extensions.

Author Contributions: Conceptualization, L.S. and J.W.; methodology, L.S. and J.W.; software, L.S.; validation, L.W., J.W. and Z.L.; formal analysis, L.S.; investigation, L.S. and J.W.; resources, L.W., J.W. and Z.L.; data curation, L.S., J.L.; writing—original draft preparation, L.S.; writing—review and editing, J.W.; visualization, L.S.; supervision, L.W. and Z.L.; project administration, J.W.; funding acquisition, J.W. All authors have read and agreed to the published version of the manuscript.

Funding: This research was funded by The National Key Research and Development Program of China grant number 2019YFB1706703.

Institutional Review Board Statement: Not applicable.

Informed Consent Statement: Not applicable.

Data Availability Statement: All data generated or analyzed during this study are included in this article.

Conflicts of Interest: The authors declare no conflict of interest.

Abbreviations

The following abbreviations are used in this manuscript:

CPS	cyber physical system
IM	intelligent manufacturing
ML	machine learning
RUL	remaining useful life
PHM	prognostics and health management
SPL	smart production line
DL	deep learning
CTC	critical transmission components
PEM	physics equation-based modeling
MLM	machine learning-based modeling
PE	physical equations
CNN	convolutional neural network
STFT	short time Fourier transform
WPD	wavelet packet decomposition
DMT	data matrix transformation
MSCNN	multi-scale CNN
ResNet	residual network
RBU	residual building units

References

- Liu, Y.; Peng, Y.; Wang, B.; Yao, S.; Liu, Z. Review on cyber-physical systems. *IEEE/CAA J. Autom. Sin.* **2017**, *4*, 27–40. [[CrossRef](#)]
- Ahmed, F.; Jannat, N.E.; Gavidel, S.Z.; Rickli, J.; Kim, K.Y. A Conceptual Framework for Cyber-physical System in Connected RSW Weldability Certification. *Procedia Manuf.* **2019**, *38*, 431–438. [[CrossRef](#)]
- Ahmed, F.; Jannat, N.E.; Schmidt, D.; Kim, K.Y. Data-driven cyber-physical system framework for connected resistance spot welding weldability certification. *Robot. Comput.-Integr. Manuf.* **2021**, *67*, 102036. [[CrossRef](#)]
- Chang, L.P.; Kuo, T.W.; Gill, C.; Nakazawa, J. Introduction to the special issue on real-time, embedded and cyber-physical systems. *ACM Trans. Embed. Comput. Syst.* **2014**, *13*, 1–2. [[CrossRef](#)]
- Lee, J.; Bagheri, B.; Kao, H.A. A cyber-physical systems architecture for industry 4.0-based manufacturing systems. *Manuf. Lett.* **2015**, *3*, 18–23. [[CrossRef](#)]
- Zhang, H.; Yan, Q.; Wen, Z. Information modeling for cyber-physical production system based on digital twin and automationml. *Int. J. Adv. Manuf. Technol.* **2020**, *107*, 2. [[CrossRef](#)]
- Chao, L.; Jiang, P. A cyber-physical system architecture in shop floor for intelligent manufacturing. *Procedia CIRP* **2016**, *56*, 372–377.
- Hyun-Jun, S.; Kyoung-Woo, C.; Chang-Heon, O. Svm-based dynamic reconfiguration cps for manufacturing system in industry 4.0. *Wirel. Commun. Mob. Comput.* **2018**, *2018*, 13.
- Feng, J.; Zhu, F.; Li, P.; Davari, H.; Lee, J. Development of An Integrated Framework for Cyber Physical System (CPS)-Enabled Rehabilitation System. *Int. J. Prognost. Health Manag.* **2021**, *12*. [[CrossRef](#)]
- Lee, J.; Jin, C.; Bagheri, B. Cyber physical systems for predictive production systems. *Prod. Eng.* **2017**, *11*, 155–165. [[CrossRef](#)]
- Bagheri, B.; Yang, S.; Kao, H.A.; Lee, J. Cyber-physical systems architecture for self-aware machines in industry 4.0 environment. *IFAC-PapersOnLine* **2015**, *48*, 1622–1627. [[CrossRef](#)]
- Lee, J.; Ardakani, H.D.; Yang, S.; Bagheri, B. Industrial big data analytics and cyber-physical systems for future maintenance and service innovation. *Procedia Cirp* **2015**, *38*, 3–7. [[CrossRef](#)]
- Lee, J.; Azamfar, M.; Singh, J.; Siahpour, S. Integration of digital twin and deep learning in cyber-physical systems: Towards smart manufacturing. *IET Collab. Intell. Manuf.* **2020**, *2*, 34–36. [[CrossRef](#)]
- Liu, Z.; Zhang, Z.; Xu, G.; Jin, W.; Lee, J. Design of Cyber-Physical Systems Architecture for Prognostics and Health Management of High-speed Railway Transportation Systems. *Int. J. Prognost. Health Manag.* **2018**, *9*. [[CrossRef](#)]
- Herwan, J.; Kano, S.; Oleg, R.; Sawada, H.; Kasashima, N. Cyber-physical system architecture for machining production line. *IEEE Ind. Cyber-Phys. Syst.* **2018**, *1*, 387–391.
- Bampoula, X.; Siaterlis, G.; Nikolakis, N.; Alexopoulos, K. A deep learning model for predictive maintenance in cyber-physical production systems using lstm autoencoders. *Sensors* **2021**, *21*, 972. [[CrossRef](#)] [[PubMed](#)]
- Lim, K.; Zheng, P.; Chen, C.; Huang, L. A digital twin-enhanced system for engineering product family design and optimization. *J. Manuf. Syst.* **2020**, *57*, 82–93. [[CrossRef](#)]
- Pandey, A.; Sequeria, R.; Kumar, P.; Kumar, S. A multistage deep residual network for biomedical cyber-physical systems. *IEEE Syst. J.* **2019**, *14*, 1953–1962. [[CrossRef](#)]
- Wasim, M.; Ahmed, I.; Ahmad, J.; Hassan, M. A Novel Deep Learning Based Automated Academic Activities Recognition in Cyber-Physical Systems. *IEEE Access* **2021**, *9*, 63718–63728. [[CrossRef](#)]

20. Zhou, X.; Xu, X.; Liang, W.; Zeng, Z.; Shimizu, S.; Yang, L.; Jin, Q. Intelligent small object detection based on digital twinning for smart manufacturing in industrial CPS. *IEEE Trans. Ind. Inf.* **2021**, *99*, 1.
21. Wu, Z.; Guo, Y.; Lin, W.; Yu, S.; Ji, Y. A weighted deep representation learning model for imbalanced fault diagnosis in cyber-physical systems. *Sensors* **2018**, *18*, 1096. [[CrossRef](#)]
22. Fei, X.; Shah, N.; Verba, N.; Chao, K.M.; Sanchez-Anguix, V.; Lewandowski, J. CPS data streams analytics based on machine learning for Cloud and Fog Computing: A survey. *Future Gener. Comput. Syst.* **2018**, *90*, 435–450. [[CrossRef](#)]
23. Dreossi, T.; Donzé, A.; Seshia, S.A. Compositional falsification of cyber-physical systems with machine learning components. *J. Autom. Reason.* **2019**, *63*, 1031–1053. [[CrossRef](#)]
24. Subramanian, M.; Skoogh, A.; Salomonsson, H.; Bangalore, P.; Bokrantz, J. A data-driven algorithm to predict throughput bottlenecks in a production system based on active periods of the machines. *Comput. Ind. Eng.* **2018**, *125*, 533–544. [[CrossRef](#)]
25. Chen, B.; Liu, Y.; Zhang, C.; Wang, Z. Time series data for equipment reliability analysis with deep learning. *IEEE Access* **2020**, *8*, 105484–105493. [[CrossRef](#)]
26. Ebrahimpour, V.; Najjarbashi, A.; Shekhalishahi, M. Multi-objective modeling for preventive maintenance scheduling in a multiple production line. *J. Intell. Manuf.* **2015**, *26*, 111–122. [[CrossRef](#)]
27. Zhang, Y.; Cheng, Y.; Wang, X.; Zhong, R.; Zhang, Y.; Tao, F. Data-driven smart production line and its common factors. *Int. J. Adv. Manuf. Technol.* **2019**, *103*, 1211–1223. [[CrossRef](#)]
28. Henriquez, P.; Alonso, J.B.; Ferrer, M.A.; Travieso, C.M. Review of automatic fault diagnosis systems using audio and vibration signals. *IEEE Trans. Syst. Man Cybern. Syst.* **2014**, *44*, 642–652. [[CrossRef](#)]
29. Xiao, D.; Huang, Y.; Zhang, X.; Shi, H.; Liu, C.; Li, Y. Fault diagnosis of asynchronous motors based on LSTM neural network. *PHM-Chongqing* **2018**, *2018*, 540–545.
30. Kang, Z.; Catal, C.; Tekinerdogan, B. Remaining useful life (RUL) prediction of equipment in production lines using artificial neural networks. *Sensors* **2021**, *21*, 932. [[CrossRef](#)]
31. Ayvaz, S.; Alpay, K. Predictive maintenance system for production lines in manufacturing: A machine learning approach using IoT data in real-time. *Expert Syst. Appl.* **2021**, *173*, 114598. [[CrossRef](#)]
32. Kang, Z.; Catal, C.; Tekinerdogan, B. Machine learning applications in production lines: A systematic literature review. *Comput. Ind. Eng.* **2020**, *149*, 106773. [[CrossRef](#)]
33. Li, T.; Zhao, Z.; Sun, C.; Yan, R.; Chen, X. Adaptive channel weighted CNN with multisensor fusion for condition monitoring of helicopter transmission system. *IEEE Sens. J.* **2020**, *20*, 8364–8373. [[CrossRef](#)]
34. Meng, T.; Jing, X.; Yan, Z.; Pedrycz, W. A survey on machine learning for data fusion. *Inf. Fusion* **2020**, *57*, 115–129. [[CrossRef](#)]
35. Rai, R.; Sahu, C.K. Driven by data or derived through physics? A review of hybrid physics guided machine learning techniques with cyber-physical system (CPS) focus. *IEEE Access* **2020**, *8*, 71050. [[CrossRef](#)]
36. Kang, T.; Cao, H.R. Dynamic prediction method for machine tool spindle rotational accuracy under cutting condition. *J. Mech. Eng.* **2020**, *56*, 9.
37. Tang, S.; Yuan, S.; Zhu, Y. Data preprocessing techniques in convolutional neural network based on fault diagnosis towards rotating machinery. *IEEE Access* **2020**, *8*, 149487. [[CrossRef](#)]
38. Zhao, Z.; Li, T.; Wu, J.; Sun, C.; Chen, X. Deep learning algorithms for rotating machinery intelligent diagnosis: An open source benchmark study. *ISA Trans.* **2020**, *107*, 224–255. [[CrossRef](#)] [[PubMed](#)]
39. Krizhevsky, A.; Sutskever, I.; Hinton, G.E. Imagenet classification with deep convolutional neural networks. *Adv. Neural Inf. Process. Syst.* **2012**, *25*, 1097–1105. [[CrossRef](#)]
40. Farabet, C.; Couprie, C.; Najman, L.; LeCun, Y. Learning hierarchical features for scene labeling. *IEEE Trans. Pattern Anal. Mach. Intell.* **2012**, *35*, 1915–1929. [[CrossRef](#)]
41. Hirschberg, J.; Manning, C.D. Advances in natural language processing. *Science* **2015**, *349*, 261–266. [[CrossRef](#)]
42. Sun, S.; Luo, C.; Chen, J. A review of natural language processing techniques for opinion mining systems. *Inf. Fusion* **2017**, *36*, 10–25. [[CrossRef](#)]
43. Lecun, Y.; Bottou, L. Gradient-based learning applied to document recognition. *Proceed. IEEE* **1998**, *86*, 2278–2324. [[CrossRef](#)]
44. Wu, C.; Yang, S.; Huang, H.; Gu, X.; Sui, Y. An improved fault diagnosis method of rolling bearings based on LeNet-5. *J. Vibrot. Shock* **2021**, *12*, 55–61.
45. Szegedy, C.; Vanhoucke, V.; Ioffe, S.; Shlens, J.; Wojna, Z. Rethinking the Inception Architecture for Computer Vision. In Proceedings of the IEEE Conference on Computer Vision and Pattern Recognition, Las Vegas, NV, USA, 27–30 June 2016; Volume 2016, pp. 2818–2826.
46. Jiang, G.; He, H.; Yan, J.; Xie, P. Multiscale convolutional neural networks for fault diagnosis of wind turbine gearbox. *IEEE Trans. Ind. Electron.* **2018**, *66*, 3196–3207. [[CrossRef](#)]
47. Chen, J.; Huang, R.; Zhao, K.; Wang, W.; Liu, L.; Li, W. Multiscale Convolutional Neural Network with Feature Alignment for Bearing Fault Diagnosis. *IEEE Trans. Instrum. Meas.* **2021**, *70*, 1–10. [[CrossRef](#)]
48. Zhao, M.; Kang, M.; Tang, B.; Pecht, M. Multiple wavelet coefficients fusion in deep residual networks for fault diagnosis. *IEEE Trans. Ind. Electron.* **2018**, *66*, 4696–4706. [[CrossRef](#)]
49. Cubillo, A.; Perinpanayagam, S.; Esperon-Miguez, M. A review of physics-based models in prognostics: Application to gears and bearings of rotating machinery. *Adv. Mech. Eng.* **2016**, *8*, 1–21. [[CrossRef](#)]

50. Liang, C.; Chen, C. Generalized Composite Multiscale Diversity Entropy and Its Application for Fault Diagnosis of Rolling Bearing in Automotive Production Line. *IEEE Access* **2021**, *9*, 84545–84558. [[CrossRef](#)]
51. Abe, K.; Matsui, G.; Tadakuma, K.; Yamano, M.; Tadakuma, R. Development of the omnidirectional transporting table based on omnidirectional driving gear. *Adv. Robot.* **2020**, *34*, 358–374. [[CrossRef](#)]
52. Zuo, Y.; Wang, H.; Wu, G.; Gu, Y.; Qiao, W. Research on remote state monitoring and intelligent maintenance system of CNC machine tools. *J. Eng.* **2019**, *23*, 8671–8675. [[CrossRef](#)]
53. Lee, J.D.; Tsai-Lin, C.W.; Lee, Y.C.; Liu, M.C.; Chen, L.Y. Fully automatic CNC machining production system. *MATEC Web Conf.* **2017**, *108*, 04002. [[CrossRef](#)]
54. Wang, L.P.; Zhang, B.B.; Wu, J. Rotation accuracy evaluation of electric spindle based on least square method. *Manuf. Technol. Mach. Tool* **2018**, *2*, 54–60.
55. Wang, L.P.; Zhao, Q.Z.; Zhang, B.B. Accuracy of an electric spindle. *Accur. Electr. Spind. Qinghua Daxue Xuebao/J. Tsinghua Univ.* **2018**, *58*, 746–751.
56. Anandan, K.P.; Ozdoganlar, O.B. A multi-orientation error separation technique for spindle metrology of miniature ultra-high-speed spindles. *Precis. Eng.* **2016**, *43*, 119–131. [[CrossRef](#)]
57. Xi, S.; Cao, H.; Chen, X. Dynamic modeling of spindle bearing system and vibration response investigation. *Mech. Syst. Signal Process.* **2019**, *114*, 486–511. [[CrossRef](#)]
58. Urbanek, J.; Barszcz, T.; Strączkiewicz, M.; Jablonski, A. Normalization of vibration signals generated under highly varying speed and load with application to signal separation. *Mech. Syst. Signal Process.* **2017**, *82*, 13–31. [[CrossRef](#)]
59. Jia, Y.; Li, G.; Dong, X.; He, K. A novel denoising method for vibration signal of hob spindle based on EEMD and grey theory. *Measurement* **2021**, *169*, 108490. [[CrossRef](#)]
60. Chen, D.W.; Wu, J.; Zhang, B.B.; Wang, L.P.; Liang, J.H. Load spectrum compilation for machining center spindles based on S-shaped specimens. *J. Tsinghua Univ.* **2018**, *58*, 1107–1114.
61. Chen, Z.; Wu, M.; Zhao, R.; Guretno, F.; Yan, R.; Li, X. Machine remaining useful life prediction via an attention-based deep learning approach. *IEEE Trans. Ind. Electron.* **2020**, *68*, 2521–2531. [[CrossRef](#)]
62. Li, K.; Ping, X.; Wang, H.; Chen, P.; Cao, Y. Sequential fuzzy diagnosis method for motor roller bearing in variable operating conditions based on vibration analysis. *Sensors* **2013**, *13*, 8013–8041. [[CrossRef](#)] [[PubMed](#)]
63. Shao, S.; McAleer, S.; Yan, R.; Baldi, P. Highly accurate machine fault diagnosis using deep transfer learning. *IEEE Trans. Ind. Inf.* **2018**, *15*, 2446–2455. [[CrossRef](#)]
64. Han, Y.; Tang, B.; Deng, L. An enhanced convolutional neural network with enlarged receptive fields for fault diagnosis of planetary gearboxes. *Comput. Ind.* **2019**, *107*, 50–58. [[CrossRef](#)]
65. He, K.; Zhang, X.; Ren, S.; Sun, J. Deep residual learning for image recognition. In Proceedings of the IEEE Conference on Computer Vision and Pattern Recognition, Las Vegas, NV, USA, 27–30 June 2016; Volume 2016, pp. 770–778.